Time Domain Synthesis of Pulsed Arrays

Matteo Ciattaglia and Gaetano Marrocco, *Member, IEEE*

***Abstract*—Pulsed arrays are becoming popular in new ultra-wideband applications to enhance the robustness of transmitted and received signals in complex environments and to identify the angle of arrival of multiple echoes. A global synthesis technique is here proposed to shape the array field in accordance to given angle-time constraints. The synthesis problem is cast as the inverse Radon transform of a desired array mask, applying the alternate projections method to include constraints over the input signals' waveform and to improve the synthesis robustness. The unknown array currents are generated as linear combinations of Hermite–Rodriguez functions in order to achieve a simple and realizable beamforming network. The effectiveness of the method is demonstrated by many examples.**

***Index Terms*—Alternate projections, array synthesis, pulsed arrays, Radon transform, space-time beamforming, ultrawideband (UWB) antennas.**

I. Introduction

ULTRAWIDEBAND (UWB) pulsed arrays [1]–[3] consist of an arrangement of antennas having more than 25% bandwidth, which are sourced by baseband carrier-free input signals. Several applications of UWB arrays have been recently proposed for communications, radar, precise indoor positioning and tracking [4]–[6].

As discussed in recent theoretical investigations, the interest in the UWB arrays relies on their unique features of grating lobe cancellation [7], sparse array design [8] and mutual coupling reduction [9]. Actual applications of pulsed arrays mainly adopt excitation scheme borrowed from narrow-band arrays: Gaussian, modulated Gaussian or Hermite-Rodriguez (HR) pulses are weighted and delayed [10] with the main objective to produce a frequency-independent beam steering. Nevertheless unconventional performance could be pursued by actual and future UWB arrays whether both the angular and the temporal dimensions were fully exploited to shape, discriminate or multiply the transmitted or radiated pulses. Pulsed radiation phenomenology in fact differs from the conventional narrow-band one, since the temporal domain, replacing the frequency domain, adds a new degree of freedom to array excitation design: the input signals' waveform.

Manuscript received August 1, 2007; revised February 26, 2008. Published July 7, 2008 (projected).

M. Ciattaglia is with the Dipartimento di Informatica, Sistemi e Produzione, University of Roma "Tor Vergata," Rome-00133, Italy, and also with SELEX SI, 00131 Roma, Italy.

G. Marrocco is with the Dipartimento di Informatica, Sistemi e Produzione, University of Roma "Tor Vergata," Rome-00133, Italy (e-mail: marrocco@disp.uniroma2.it).

Color versions of one or more of the figures in this paper are available online at http://ieeexplore.ieee.org.

Digital Object Identifier 10.1109/TAP.2008.924714

In the last decade, more advanced synthesis techniques have been specifically proposed for the UWB array design, even if with still limited optimization objectives.

For instance, the method in [11] is aimed to the design of sparse non-uniform arrays that realize an already known continuous source distribution with the radiation pattern constrained into a limited angular sector. In [12] two schemes are proposed for space-time shaping of an aperture distribution in order to compensate the time-derivative of the input signals, which is intrinsic in the current to far-field projection.

The two methods in [13] and [14] permit to compute, through frequency domain processing, the array input waveforms by minimization of a variational expression accounting for bandwidth constraints and inter-antenna coupling. The methods were applied to linear arrays of dipoles, to optimize the amplitude of the transient radiated field at a specified time and angular position [13], or the transmitted energy in a specified time interval [14].

A space-time beamforming technique has been recently proposed for application to UWB microwave imaging aimed to breast cancer detection [15]. The post-processing (time-delay and filtering) of the sampled signals, collected by an UWB radar, is applied to identify the presence and location of a dielectric anomaly by compensation of undesired propagation effects, artifacts and noise.

In this paper, a more general time-angle synthesis technique is introduced. Unlike the above cited methods, the proposed technique permits a full shaping of the radiated field and it is able to generate the array input signal waveforms together with the beamforming network's topology. The synthesis is formulated as an angle-time constrained inversion problem based on the fact that the time-domain antenna far field can be related to the Radon transform of the space-time-varying currents [16]. Thus, given a desired far field, for instance specified through a mask, a Radon transform [17], relating the array port currents to far field pattern, needs to be inverted to find the optimum time-domain currents waveforms. Constraints over the beamforming network are included by mapping the unknown currents onto a proper set of time-dependent basis functions. To improve the robustness and the efficiency of this idea, the constrained Radon inversion is hence performed by successive iterations within the framework of the alternating projections method, proposed in [18] for monochromatic arrays, and here extended to the time domain.

The paper is organized as follows. In Section II the time domain synthesis problem is formally introduced, then the extension to the time-domain of the alternate projection method is described in Section III, with particular attention to the inclusion of the current waveform constraints. The resulting iterative procedure is globally explained in Section VI and, finally, the applicability of the method is discussed in Section V by the help of many examples.

II. The Constrained Time Domain Synthesis Problem

Given a linear array of N elements along the z axis at positions $z_n = nd$, $(n = 1 \dots N)$ and driven by a set of inward currents $\boldsymbol{I}(t) = [i_1(t), i_2(t), \dots, i_N(t)]^T$, the time-domain array factor [7] is

$$AF(\theta, t) = \sum_{n=1}^{N} i_n(t + t_n(\theta)) \tag{1}$$

where $t_n(\theta) = n(d/c)\cos\theta$ and c is the speed of light. The mutual coupling among radiating elements is here neglected since it plays a secondary role in the case of pulsed arrays as demonstrated in [9]. All the antennas are supposed to radiate the same radiation pattern, and therefore the total radiated field of the array is the convolution between the array factor and the element effective height, [16], $\underline{h}^T$

$$\underline{E}(\theta, \phi, t) = -\frac{\eta_0}{4\pi r c}\underline{h}^T(\theta, \phi, \cdot) * AF(\theta, \cdot)\left[t - \frac{r}{c}\right] \tag{2}$$

where η_0 is the free-space impedance and "$*$" is the convolution. Let us now consider a line source $i(z,t)$ such that the array currentsI (ϵ) are obtained by sampling the line at points z_n

$$\boldsymbol{I}(t) = \boldsymbol{\Delta}_d(z) * i(z, t) \tag{3}$$

where the sampling operator is defined as

$$\boldsymbol{\Delta}_d(z) = [\delta(z - d), \delta(z - 2d), \dots, \delta(z - Nd)]. \tag{4}$$

Assume now to apply the Radon transform to $i(z,t)$

$$\mathcal{R} \circ i(z, t) = \int_{-\infty}^{+\infty} i\left(z, t + \frac{z}{c}\cos\theta\right) dz. \tag{5}$$

The resulting function has the meaning of the space factor of the continuous line source in analogy to the monochromatic regime [19]. It is easy to show that a discretization of the above integral at the array points

$$\mathcal{R} \circ i(z, t)|_{z=nd} = \sum_{n=1}^{N} i\left(nd, t + \frac{nd}{c}\cos\theta\right) d \tag{6}$$

may be related to the array factor as

$$AF(\theta, t) = \mathcal{R}_n \circ \boldsymbol{I}(t) \tag{7}$$

where the discretized Radon operator $\mathcal{R}_n$[17] is such that $\mathcal{R}_n \circ i(z,t) = 1/d\mathcal{R} \circ i(z,t)|_{z=nd}$, and may be formally defined, from (6) and (3), as

$$\begin{aligned}\mathcal{R}_n \circ &= \boldsymbol{\Delta}_{d/c\cos\theta}(\tau - t) * \\ &= \left[\delta\left(\tau - t - \frac{d}{c}\cos\theta\right), \dots, \delta\left(\tau - t - \frac{Nd}{c}\cos\theta\right)\right] *\end{aligned} \tag{8}$$

where $\mathcal{R}_n$ applies to the array currents $\boldsymbol{I}(t)$ according to the row-by-column paradigm. The functional relationships among the array currents, the array factor and the continuous line source are resumed in the graph of Fig. 1, where $\mathcal{R}^{-1}$ is the inverse Radon transform which can be computed by means of a sequence of direct and inverse Fourier transforms, via the Projection Slice Theorem, as described in Appendix.

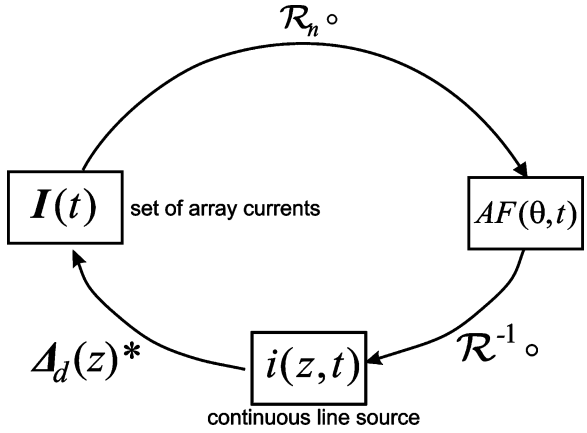

Fig. 1. Logical relationship among the array currents, the continuous-line source and the array factor.

The synthesis problem is defined as the retrieval of the excitation currents, once the array elements, the array geometry, the desired radiation pattern and some constraints over the current waveforms have been specified.

In the synthesis method here discussed, both the above continuous ($i(z,t)$) and discrete ($\boldsymbol{I}(t)$) representations of the unknown currents are employed. In particular, an iterative procedure is introduced wherein successive estimations of the continuous line source are basically produced by the inverse Radon transform of a desired pattern, while the control over the current waveforms requires the sampling of the continuous line source and the application of the $\mathcal{R}_n$ operator. Since the radiated field in (2) is obtained by a angular-temporal filtering of the array factor due to the antennas' effective height, the array pattern's time dependence is expected to be sensibly different from that of the radiated field, unlike in the monochromatic regime, and therefore it is more conservative to enforce the pattern constraints directly over the radiated field, rather than over the array factor. Without loss of generality it is additionally assumed that the array radiation requirements are specified in the far field, at $r = 1$ m and $\phi = 0°$ for notation simplicity, over the only co-polar component of the total radiated field, (say E_θ), which has to be bounded between upper and lower angle-time masks $M_u^E(\theta, t)$ and $M_l^E(\theta, t)$ so that

$$M_l^E(\theta, t) \le E_\theta(\theta, \phi, t) \le M_u^E(\theta, t). \tag{9}$$

The synthesis method will be instead referred to the array patterns masks $M_u^{AF}(\theta, t)$ and $M_l^{AF}(\theta, t)$ which, according to (2), are obtained from $M_{l,u}^E$ by means of deconvolution of the element effective height

$$M_{l,u}^{AF}(\theta, t) = -\frac{4\pi r c}{\eta_0} h_\theta^T(\theta, \cdot) \otimes M_{l,u}^E(\theta, \cdot)(t) \tag{10}$$

where $a = b \otimes c$ indicates the deconvolution of the function b out of the function c, e.g., such that $a * c = b$. Many options are available to perform such a deconvolution quickly and accurately, for instance by using least squares [20] or moment expansions algorithms [21], [22]. With more simplicity, since a relevant part of the processing may be performed in the frequency domain, through the projection slice theorem reviewed in the Appendix,

the deconvolution could be also achieved in the frequency domain as $\widetilde{M}_{l,u}^{AF}(\theta,\omega) = -4\pi rc/\eta_0 \widetilde{M}_{l,u}^{E}(\theta,\omega)/\widetilde{h}_{\theta}^{T}(\theta,\omega)$, with the tilde symbol "$\widetilde{\ }$" tagging the $t \rightarrow \omega$ Fourier transform.

The array factor and the radiated pattern corresponding, through (7) and (2), to the currents originated from the synthesis are hereafter denoted as *realized array factor* and *realized pattern*, respectively. Since the cross-polar component is neglected in the synthesis process, the term "radiated field" will refer, in the rest of the paper, to the only co-polar component.

The constrained time domain synthesis problem can be formulated in a general way as an *intersection finding* problem. Let $\mathcal{B}$ denote the set of all the array factors which can be radiated by the considered array arrangement for any choice of the input current set

$$\mathcal{B} = \left\{ AF(\theta,t) : AF(\theta,t) = \sum_{n=1}^{N} i(t + t_n(\theta)),\ \forall\ \{i(t)\} \right\}. \tag{11}$$

The constraints over the beamforming network are introduced by enforcing the array current waveforms $\boldsymbol{I}(t)$ to be linear combination of a prescribed set of K basis functions $\{w_k(t)\}$ which may be simply generated by a particular network topology. Such a constraint will therefore produce a subset $\mathcal{W} \subset \mathcal{B}$ containing the waveform-constrained array factors, generated by such antenna currents.

The constraints over the pattern shape originate a set, $\mathcal{M}$, of all the angle-time functions $g(\theta,t)$ bounded between the masks, e.g., such that

$$\mathcal{M} = \left\{ g(\theta,t) : M_l^{AF}(\theta,t) \le g(\theta,t) \le M_u^{AF}(\theta,t) \right\}. \tag{12}$$

The solution to the synthesis problem is finally an array factor which belongs to the intersection $\mathcal{W} \bigcap \mathcal{M}$.

III. Angle-Time Alternate Projections

One of the most effective methods for the solution of the intersection problem is based on the alternate projection, as in [18], which is here properly extended to time-domain arrays.

In general, a *projector* P_A over the closed subset $\mathcal{A}$ of a normed space $\mathcal{H}$ is the operator defined by

$$P_A : x \in \mathcal{H} \rightarrow y_0 \in \mathcal{A} : \|x - y_0\| \le \|x - y\|, \quad \forall\ y \in \mathcal{A}. \tag{13}$$

The point y_0, which is the point of $\mathcal{A}$ nearest to x, is called the projection of x over $\mathcal{A}$.

In the time-domain array synthesis, two projectors, applying to array factor-like functions, need to be introduced. $P_{\mathcal{M}}$ projects *waveform-constrained* array factors to the set $\mathcal{M}$ of the *mask-constrained* functions (see Fig. 2) and $P_{\mathcal{W}}$ performs the converse projection to $\mathcal{W}$. These two projections are iterated until the intersection $\mathcal{W} \bigcap \mathcal{M}$, whether existent, is found.

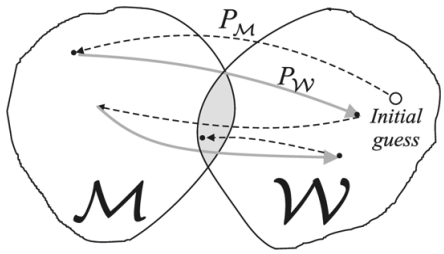

Fig. 2. Alternating projections applied between the sets $\mathcal{M}$ and $\mathcal{W}$.

A. Constraints Over the Angular Pattern: The $P_{\mathcal{M}}$ Projector

The projector $P_{\mathcal{M}}$ is defined in a conventional way as in the frequency domain and basically crops the realized array factor outside the masks: see (14) at the bottom of the page.

B. Constraints Over the Currents' Waveform: The $P_{\mathcal{W}}$ Projector

The projector $P_{\mathcal{W}}$ is instead specifically introduced for the time-domain synthesis and is given by the cascade of three operators

$$P_{\mathcal{W}} = \mathcal{R}_n \circ \mathcal{C}_w \circ \mathcal{R}^{-1} \tag{15}$$

which, as described in the graph of Fig. 1, exploits the relationship among the currents' and pattern's domains and additionally, by means of the operator C_w, enforces the required waveform constraints onto the currents. To be specific, the operator C_w applies to the actual estimation of array continuous source $i(z,t)$ and performs a two step processing: first it samples $i(z,t)$ at point $z_n = nd$, and hence maps the so produced set of N time-variant functions $\boldsymbol{I}(t)$ onto a set of K basis waveforms $\{w_k(t)\}$, useful to introduce the beamforming constraints in $\mathcal{W}$

$$\boldsymbol{I}_w(t) = C_w \circ i(z,t) = \left\{ \sum_{k=0}^{K} \alpha_{n,k} w_k(t - \tau_n) \right\}_{n=1\ldots N} \tag{16}$$

where the time shift τ_n is the barycenter of the nth current $\boldsymbol{I}(n)[t]$, required to align each array current to the HR functions which are defined symmetrically with respect to the temporal origin

$$\tau_n = \frac{\int t |i(z_n,\tau)| d\tau}{\int |i(z_n,\tau)| d\tau}. \tag{17}$$

Several families of basis functions may be applied to efficiently map a time-limited signal, and among them it is worth to mention the associate Hermite functions and the HR functions [23], [24], popular in neuroscience and in the processing of moving images, the prolate spheroidal functions [5] applied in UWB data generators, and the complex exponentials [25] useful

$$P_{\mathcal{M}} \circ AF(\theta,\cdot) = \begin{cases} M_u^{AF}(\theta,\cdot) & \text{if } |AF(\theta,\cdot)| > M_u^{AF}(\theta,\cdot) \\ AF(\theta,\cdot) & \text{if } M_l^{AF}(\theta,\cdot) < |AF(\theta,\cdot)| < M_u^{AF}(\theta,\cdot) \\ M_l^{AF}(\theta,\cdot) & \text{if } |AF(\theta,\cdot)| < M_l^{AF}(\theta,\cdot) \end{cases} \tag{14}$$

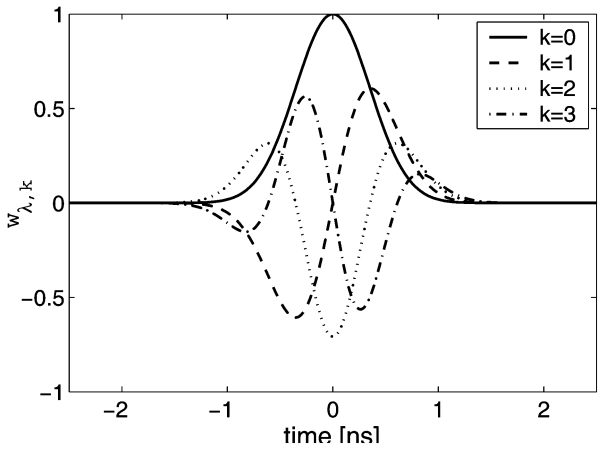

Fig. 3. HR functions of orders $k = 0$ to 3.

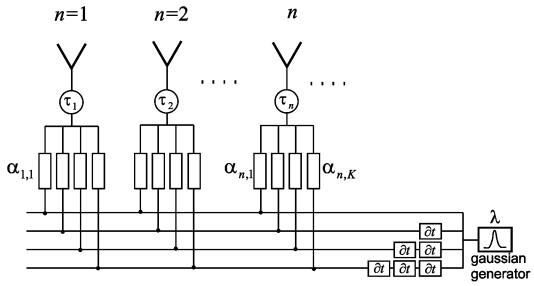

Fig. 4. A possible realization of the beamforming network as deduced from (16). The topology, here described for the particular case of $K = 4$, permits to synthetize the HR components of the input array currents. The processing modules basically comprise differentiators, attenuators and delay lines.

to fit transients. The proposed array synthesis handles the orthogonal HR functions

$$w_k(t) = \frac{1}{\sqrt{2^k k!}} H_k\left(\frac{t}{\lambda}\right) \frac{1}{\sqrt{\pi}\lambda} e^{-t^2/\lambda^2} \tag{18}$$

where λ is a scale parameter and $H_k(t)$ is the Hermite polynomial of order k. The corresponding mapping coefficients $\alpha_{n,k}$ in (16) are calculated as

$$\begin{aligned} \alpha_{n,k} &= \langle i(z_n, t+\tau_n), w_{\lambda,k}(t) \rangle \\ &= \frac{1}{\sqrt{2^k k!}} \int_{-\infty}^{+\infty} i(z_n, t+\tau_n) H_k\left(\frac{t}{\lambda}\right) dt. \end{aligned} \tag{19}$$

The HR functions are successive differentiation of a Gaussian pulse (Fig. 3) and hence they may be simply generated by a beamforming network topology (see Fig. 4 for one of the possible realizations) comprising a single Gaussian pulse generator with parameter λ, plus modules performing derivatives, attenuation and delay.

The complexity of the network, e.g., the number of processing modules, can be *a priori* defined by the mapping order K, which corresponds to enforce a topology constraint onto the beamforming scheme. The choice of K fixes the degrees of freedom of the network and affects the speed and the quality of the achieved results. A small K means a hard constraint over the currents' waveform and the intersection finding problem could not find a solution, even with a large number of radiating elements.

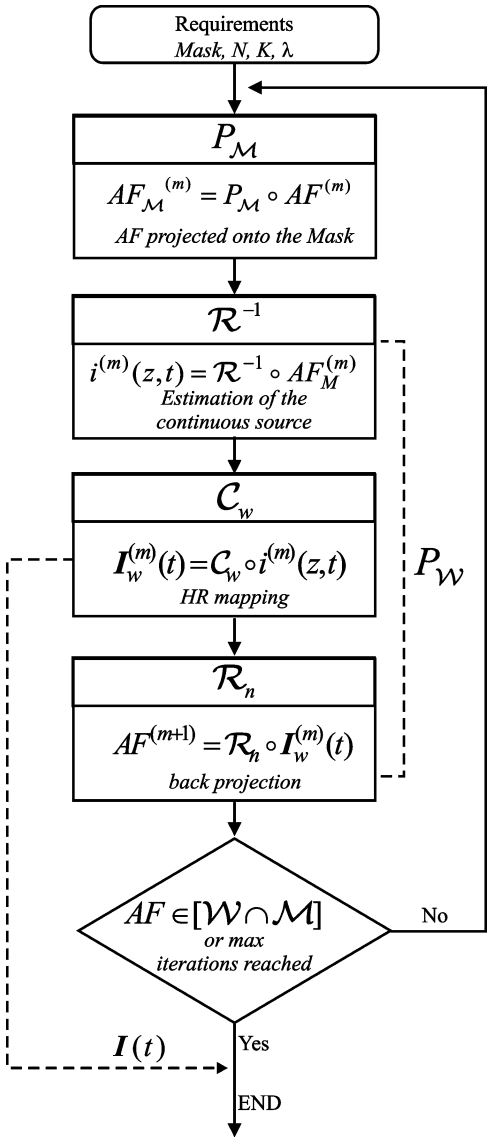

Fig. 5. Flow chart of the presented synthesis method.

The mapping in (16) is sensitive to the scale parameter λ which could be either fixed *a priori* by the required beamforming network topology, or automatically deduced by the synthesis itself, starting from the time duration of the mth estimation of the array currents. According to our experience, the first choice appears more robust and permits an external tuning of the accuracy. Further discussion and guidelines for the choice of λ and K will be given in the numerical example section.

IV. Iterative Procedure

With reference to the flowchart in Fig. 5, the synthesis procedure begins with an initial guess for the array factor, for instance the defined upper mask $M_u^{AF}(\theta, t)$. The first step $(m = 1)$ of the synthesis thus performs a simple Radon inversion of the starting guess pattern with a proper mapping of the excitations

$$\boldsymbol{I}_w^{(1)}(t) = C_w \circ \mathcal{R}^{-1} \circ M_u^{AF}(\theta, t) \tag{20}$$

Then, a new iteration $(m = 2)$ is generated by the evaluation of the realized array factor $AF^{(2)} = \mathcal{R}_n \circ \boldsymbol{I}_w^{(1)}(t)$, and the iterative application of the two projectors $P_{\mathcal{M}}$ and $P_{\mathcal{W}}$ produces the successive mth estimations of the source

$$i^{(m)}(z,t) = \mathcal{R}^{-1} \circ [P_{\mathcal{M}} \circ AF^{(m)}(\theta,t)] \tag{21}$$

while $\boldsymbol{I}_w^{(m)}(t) = C_w \circ i^{(m)}(z,t)$ gives their projection onto the allowed HR waveform domain. The procedure terminates when either the convergence is achieved, e.g., the resulting array pattern falls into the intersection $\mathcal{W} \bigcap \mathcal{M}$, or a maximum number of iterations have been reached. In any case, the iterative procedure inherits the convergence's features of the more conventional frequency domain alternate projections schemes and in particular the optimal solution could be not found if the two sets $\mathcal{M}$ and $\mathcal{W}$ are disjoined due to excessively hard requirements compared with the available degrees of freedom.

V. Numerical Examples

The performances of the proposed time-domain synthesis are here discussed by means of some examples involving monocycles and multiple-monocycle pulses. The co-polar component of the element's effective height was supposed to be

$$h_\theta^T(\theta,t) = \delta^{(q)}(\tau)\cos^p\theta \tag{22}$$

where the $\delta^{(q)}$ produces the qth derivative of the input signals and the superscript "p" modulates the antenna's angular beamwidth. This canonical representation of the element factor greatly simplifies the deconvolution in (10) which is hence achieved by numerical integration of the given masks over the time. It is worth noticing that the case $q = 1$ (ideal differentiator) is a good model for true UWB antennas, the case $q = 2$ represents the response of a small dipole [16] and, finally, $q = 3$ close resembles the impulse response of moderately large-band antennas such as a diamond dipole [26].

The masks are given in the form of rectangular windows as in Fig. 6. The parameters are the pulse duration T, the angular beamwidth Θ, the tilt angle θ_0, the time delay t_0, the main lobe amplitudes M_0, M_1, the side lobe level M_{SL} and time and angular transition ΔT and $\Delta\Theta$.

The size of the array, as well as the number of antennas, are related to the angular and temporal size of the desired field mask. Following the discussion in [27], within the simplified hypothesis of an array whose antennas radiate identical rectangular-pulse-like waveforms, the angular beamwidth of a pulsed arrays referred to the peak value can be expressed as

$$\Theta = \frac{2-e}{e}\frac{2cT}{L} \tag{23}$$

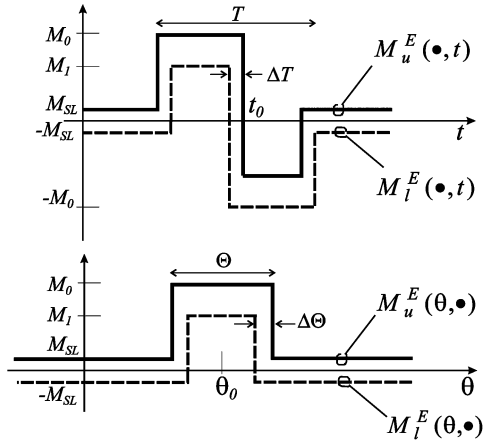

Fig. 6. Rectangular-pulse-like mask applied in the examples.

where $L = Nd$ is the array length, and e is the reference attenuation of the field with respect to the maximum, as considered to apply the beamwidth definition. For rectangle-like masks, as those used in this paper, it is assumed $e = 1$. A first estimation of the array geometry, starting from a mask with overall time-angular size $T \times \Theta$, is then

$$Nd = \frac{2cT}{\Theta} \tag{24}$$

with array spacing $d < cT$ to avoid grating lobes [7]. We moreover verified that the choice $d < cT/2$ permits to reduce the strength of side lobes.

The time-duration (support) of the mask suggests the selection of the scaling factor λ in the HR processing. According to the recommendation in [23], λ is chosen as a fraction of the support of the mask waveform to be synthesized. In most of the proposed examples we will generally set $\lambda = 0.4$ T, except for when differently specified.

The following parameters are fixed: $p = 1$, $M_0 = 1$, $M_1 = 0.7$, $M_{SL} = 0.1$, while the beamforming network order K, the array spacing d, the number of elements and the antenna order q, will be changed to check the method. The convergence of the synthesis, e.g., the difference between the realized field and the mask is quantified by a L^2 norm which gives the distance of the realized field from the mask, shown in (25) at the bottom of the page, where $E^{(m)}(\theta,t)$ indicates the realized array field at the mth iteration evaluated at point $r = 1$ m and $\phi = 0°$, the selectors $\xi_{u,l}(\theta,t)$ are defined as

$$\begin{aligned}\xi_u(\theta,t) &= \begin{cases} 1, & E^{(m)}(\theta,t) > M_u^E(\theta,t) \\ 0, & \text{otherwise} \end{cases} \\ \xi_l(\theta,t) &= \begin{cases} 1, & E^{(m)}(\theta,t) < M_l^E(\theta,t) \\ 0, & \text{otherwise.} \end{cases}\end{aligned} \tag{26}$$

$$\varepsilon(m) = \sqrt{\frac{\int\int \left[\left|E^{(m)}(\theta,t) - M_u^{AF}(\theta,t)\right|^2 \xi_u(\theta,t) + \left|E^{(m)}(\theta,t) - M_l^{AF}(\theta,t)\right|^2 \xi_l(\theta,t)\right] d\theta dt}{\int\int \left|M_u^E(\theta,t)\right|^2 d\theta dt}} \tag{25}$$

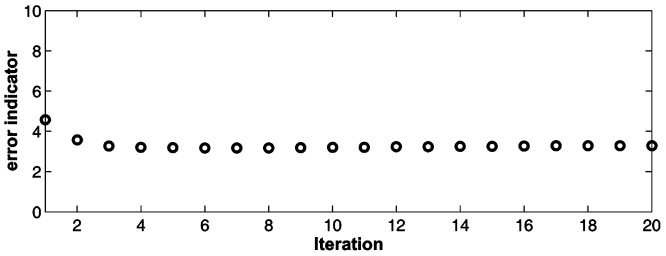

Fig. 7. Broadside monocycle $(\Theta, t) = (30°, 1\ \mathrm{ns})$—synthesis set-up: $d = 10\ \mathrm{cm}$, $N = 12$, $K = 1$, $q = 1$. Convergence indicator $\varepsilon(m)$.

Moreover, to better discuss the results, the final realized field and the realized currents will be also observed through the *energy detector* and the *r.m.s. time width detector*

$$\tilde{E}(\theta) = \|E(\theta, t)\|_2 \tag{27}$$

$$\tilde{\imath}_n = \|\boldsymbol{I}_w(n)[t]\|_2, \quad n = 1 \ldots N \tag{28}$$

$$T_n = \frac{\|t\boldsymbol{I}_w(n)[t - \tau_n]\|_2}{\|\boldsymbol{I}_w(n)[t]\|_2}, \quad n = 1 \ldots N. \tag{29}$$

A. Broadside Single Monocycle Pulse

A first application of the synthesis considers a rather coarse mask with $\Theta = 30°$, $\theta_0 = 0°$, $T = 1\ \mathrm{ns}$, $t_0 = 1.5\ \mathrm{ns}$, $\Delta T = 40\ \mathrm{ps}$ and $\Delta\Theta = 5°$ in the scheme of Fig. 6. From (24) the estimated array length is $L = 1.15\ \mathrm{m}$ and having fixed the array spacing $d = 10\ \mathrm{cm}$ ($< cT/2 = 15\ \mathrm{cm}$), the array elements is $N = 12$. The radiators are ideal antennas [$q = 1$ in (22)] and the beamforming network preliminary comprises only Gaussian and derivated-Gaussian pulses $(K = 1)$.

The optimization procedure is stable (Fig. 7) and indistinguishable results are generally achieved, in these and in most of the following tests, just after 5–10 iterations.

It is worth noticing in Fig. 8 that the actual choice of K is not adequate to match the mask. In particular, as visible in the chart of the beamforming coefficients $\{\alpha_{n,k}\}$, the realized field is mainly produced by the first derivative of the HR function $w_1(t)$ which gives relevant contribution outside the mask. Much better results are instead achieved by considering the same configuration as before but with a beamforming order $K = 8$ (Fig. 9). In this case the synthesis selects even waveforms, and coefficients $\alpha_{n,2}$, $\alpha_{n,4}$ are the most excited. The realized field is now better angularly collimated and the time-spread outside of the mask is sensibly reduced.

By increasing the array length to $L = 1.75\ \mathrm{m}$, and especially by reducing the inter-element spacing to $d = 5\ \mathrm{m}$ $(N = 35)$, the realized field is really well matched to the mask (Fig. 10). In spite of the simple desired field, the realized input antenna currents are greatly different in their transient shape, depending on the position into the array. It is interesting to analyze the energy $\tilde{\imath}_n$ and the r.m.s. time duration T_n of such currents (Fig. 10 bottom), as defined in (28) and (29). The energy tapering from the middle to the edges of the array is required for angular collimation and to reduce the sidelobes, as in the monochromatic regime. The converse tapering in the r.m.s. time width from the

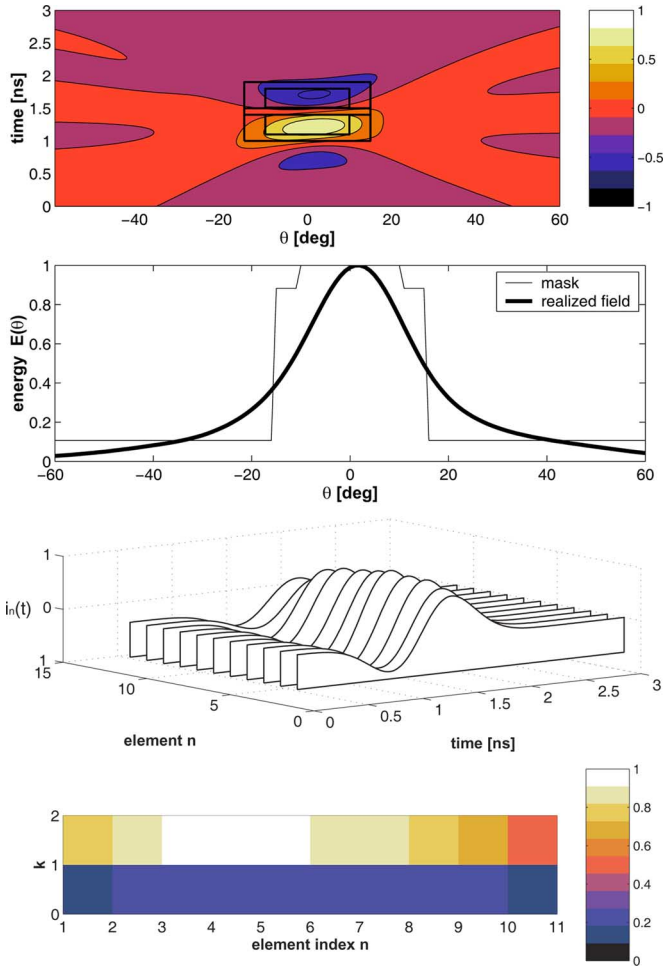

Fig. 8. Broadside monocycle $(\Theta, t) = (30°, 1\ \mathrm{ns})$—synthesis set-up: $d = 10\ \mathrm{cm}$, $N = 12$, $K = 1$, $q = 1$. From top to bottom: realized field pattern, field energy $\tilde{E}(\theta)$, realized currents and corresponding beamforming coefficients $\{\alpha_{n,k}\}$.

edges to the middle of the array is in close agreement with the theory of iso-diffracting apertures [12]. Such a theory indicates that the maximum angular frequency $\omega_{\max}(z)$ (proportional to $1/T_n$) of the aperture signals, and hence of the corresponding array currents, has to decrease from the center to the edge in order to produce space-time collimated beams, as found in the considered example.

B. Highly Collimated and Steered Monocycle

An example of $\Theta = 5°$ collimated beam $(\Delta\Theta = 2°)$ is here reported. By setting the array spacing to $d = 10\ \mathrm{cm}$, the estimated radiators' number is $N = 65$. The beamforming network order is fixed to $K = 6$. The very first iteration of the synthesis process (Fig. 11 top), which is formally the inverse Radon Transform of the desired mask projected onto the HR space [see (20)], yields a realized field distribution collimated in the angle but completely un-synchronized to the time behavior of the mask. At the 10th iteration, after that the convergence indicator remains unchanged, the realized field is well constrained into the mask with only a few residual side contribution of low strength in the surrounding of the beam.

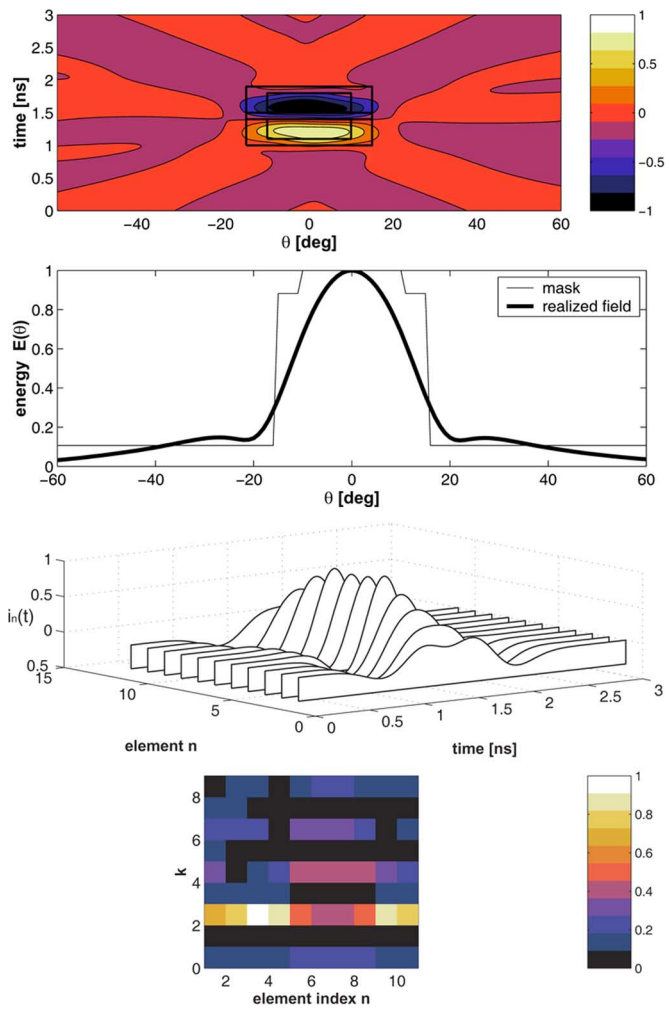

Fig. 9. Broadside monocycle $(\Theta, t) = (30°, 1\ \mathrm{ns})$—Synthesis set-up as in Fig. 8 except for $K = 8$.

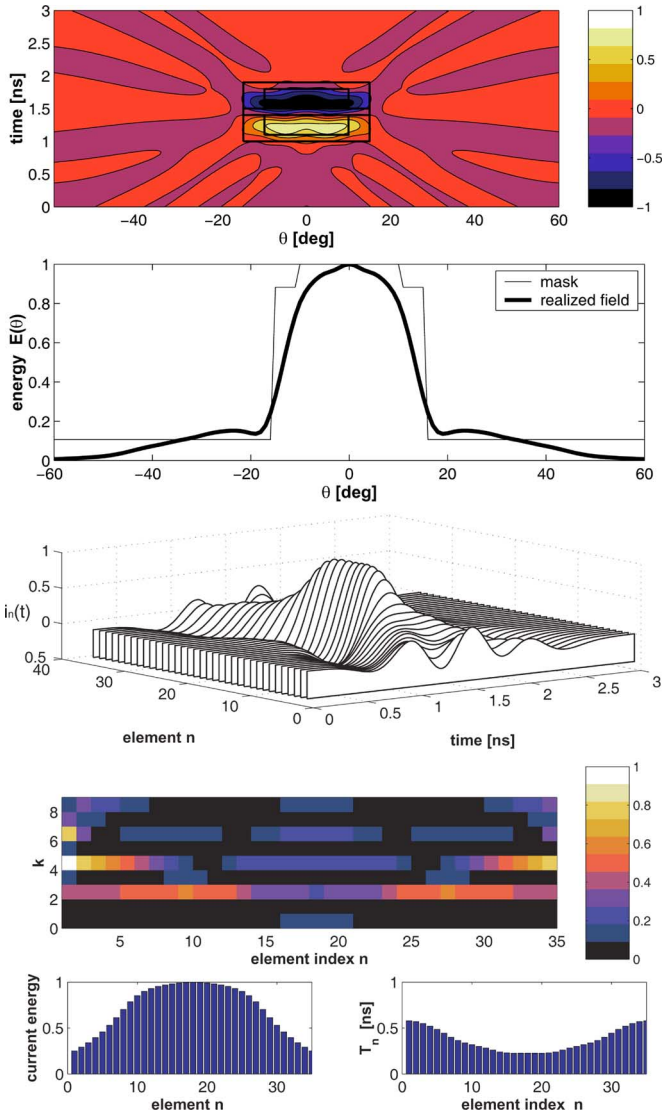

Fig. 10. Broadside monocycle $(\Theta, t) = (30°, 1\ \mathrm{ns})$—Synthesis set-up as in Fig. 8 except for $d = 5\ \mathrm{cm}$, $N = 35$ and $K = 8$. The last row shows the energy i_n and the r.m.s. time width T_n indicators of the realized currents.

The same mask of the previous example is now steered to an angle of $\theta_0 = 10°$. The results in Fig. 12 show a similar pattern as before, with a progressive time shift of the array current waveforms depending on each radiating element position, in order to have the beam tilted to the desired angle.

C. Higher Order Antennas

The synthesis algorithm is now applied to a less ideal antenna, by assuming a high-order derivative $q = 3$ in the impulse response model (22), which is now representative of a broadband planar dipole such as the bowtie or the diamond. The field mask is the same as in the highly collimated example with $\Theta = 5°$, $T = 1\ \mathrm{ns}$, and the array geometry is again $d = 10\ \mathrm{cm}$ and $N = 65$. Since the deconvolution is a commutative operator, the effect of higher-order derivative in (22) is expected to propagate up to the HR functions, reducing the maximum order of the excited waveform, since $\delta^{(q)}(t) \otimes w_k(t) = w_{k-q}(t)$. Therefore the optimization will be performed with a low-order beamforming network, $K = 3$ in the specific. By numerical experiments it was found that best results are achieved if the scaling factor λ is larger than in the $q = 1$ examples and, in particular, the choice $\lambda = 0.7\ \mathrm{T}$ is considered.

The synthesis procedure is stable also in this case after about the 10th iterations (Fig. 13) and the diagrams in Fig. 14 show results comparable with that of an ideal antenna (see Fig. 11 for comparison) even if some additional time-oscillations outside the mask make the time collimation an harder goal to achieve. It is also interesting to note that the array elements are nearly excited with the same waveforms and, as expected from the above discussion, also the lowest-order HR-functions $w_0(t)$ are fully excited. We have verified that more complicated beamforming networks $(K > 3)$ do not improve further the results. Finally, not reported experiments for the $q = 2$ case have shown similar results provided that $\lambda = 0.6\ \mathrm{T}$.

D. Multibeam Pattern

A more challenging field mask (Fig. 15) includes two independent beams $(\Theta_1 = \Theta_2 = 30°, \theta_{01} = -\theta_{02} = -30°$, $T_1 = 1.1\ \mathrm{ns}$, $T_2 = 9.9\ \mathrm{ns})$ with different waveforms radiated

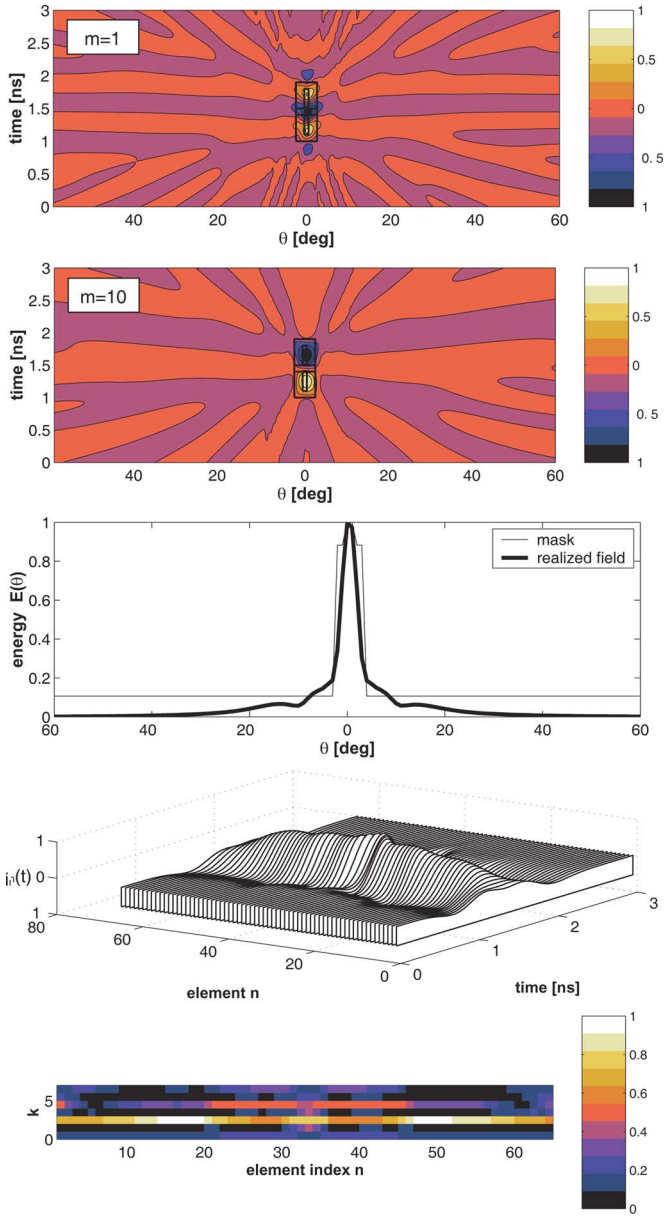

Fig. 11. Highly collimated monocycle $(\Theta, T) = (5^\circ, 1\,\mathrm{ns})$—Synthesis set-up: $d = 10$ cm, $N = 65$, $K = 6$, $q = 1$. From top to bottom: realized field at the first $(m = 1)$ iteration; realized field and related currents at steady state $(m = 10)$ iteration.

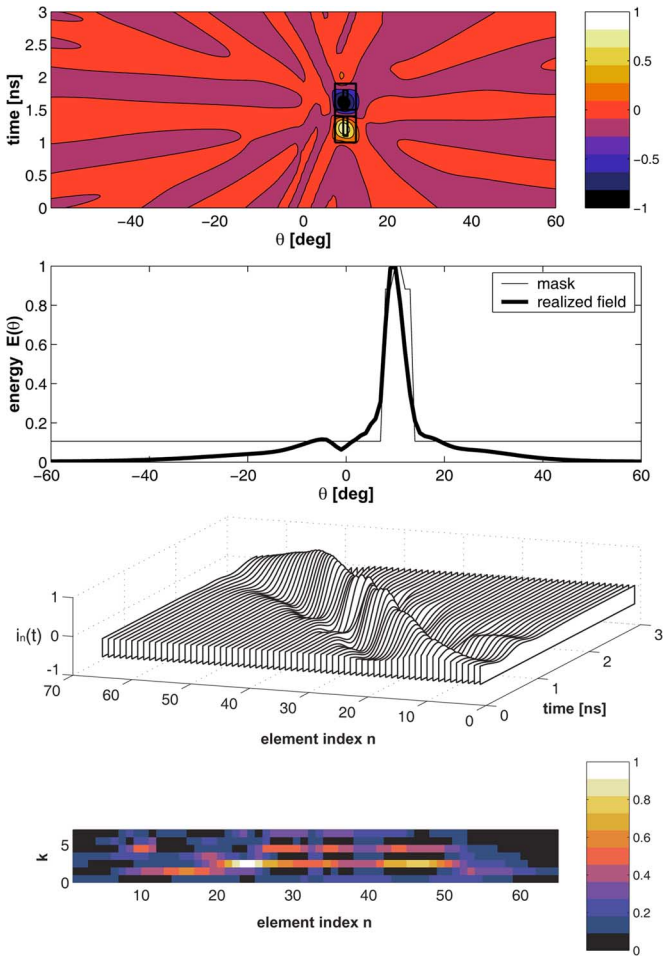

Fig. 12. Steered collimated monocycle $(\Theta, T) = (5^\circ, 1\,\mathrm{ns})$—Synthesis set-up as in the previous example but with an angular steering to $\theta_0 = 10^\circ$.

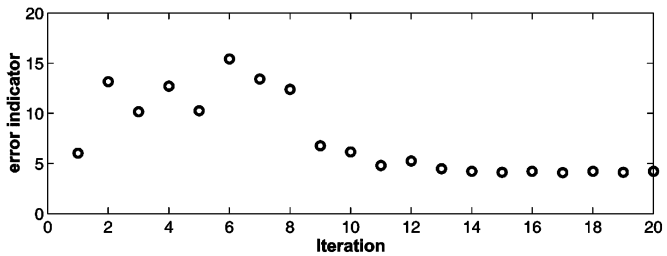

Fig. 13. Higher-order antennas $\delta^{(3)}(t)$; $(\Theta, T) = (5^\circ, 1\,\mathrm{ns})$—Synthesis set-up: $d = 10$ cm, $N = 65$, $K = 3$, $q = 3$, $\lambda = 0.7$ T. Convergence indicator $\varepsilon(m)$.

along the two angular directions: three oscillations in the first beam and two oscillations in the other one.

The scale parameters λ is now set to $\lambda = 0.55T_1$ and the estimated array length is $L = Nd = 1.25$ m. Having set $d = 5$ cm, the element number is chosen as $N = 40$ [the minimum required by guidelines in (24) should be (25)]. The realized field and currents at the steady state (after 5 iterations) are shown in Fig. 16 for a beamforming network order $K = 14$. The two different waveforms are clearly recognized, even with a few out-of-the-mask oscillations. The array currents are now rather irregular, and each waveform exhibits a different temporal behavior. The beamforming coefficients matrix is much denser than in the previous examples, with some predilection for the right side because of the asymmetry of the desired pattern.

The shape of the currents may be explained if we consider two other array synthesis problems wherein, under the same conditions as before, each beam is independently optimized (Fig. 17). The corresponding currents show the typical uniform delay (opposite in the two cases) required to steer the beams. It can be figured out that the superposition of such currents gives the diagram of the true multibeam design and this is an interesting results since the synthesis method, in the multibeam case, has required half the time of two mono-beam optimizations.

VI. Conclusion

The proposed method gives the full control over the array pattern in both the angular and time domains. Real antennas can be

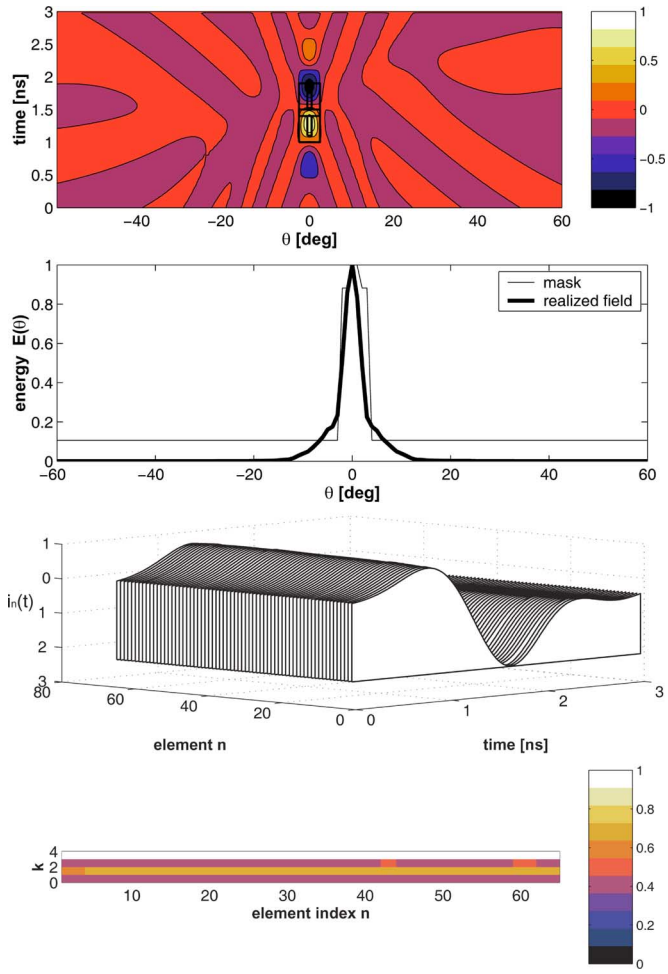

Fig. 14. Higher-order antennas $\delta^{(3)}(t)$; $(\Theta, T) = (5°, 1\ \text{ns})$—Synthesis set-up: $d = 10\ \text{cm}$, $N = 65$, $K = 3$, $q = 3$, $\lambda = 0.7\ \text{T}$. Realized field and currents.

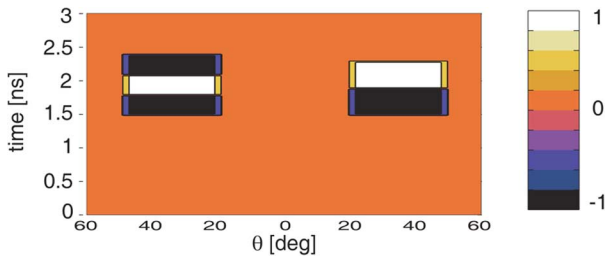

Fig. 15. Multibeam pattern: $\Theta_1 = \Theta_2 = 30°$, $\theta_{01} = -\theta_{02} = -30°$, $T_1 = 1.1\ \text{ns}$, $T_2 = 0.9\ \text{ns}$.

taken into account through their simulated or measured effective height as well as by means of analytic fitting expressions.

The synthesis scheme enables a great flexibility to suite a particular beamforming network. The proposed guidelines permits to simply set all the signal and geometrical parameters depending on the enforced mask.

The described formulation, involving the HR functions, is just one of the possible options and it can be easily extended to other set of waveforms, even belonging to heterogenous families. In such a case the mapping operator C_w should generally perform a best fitting operation.

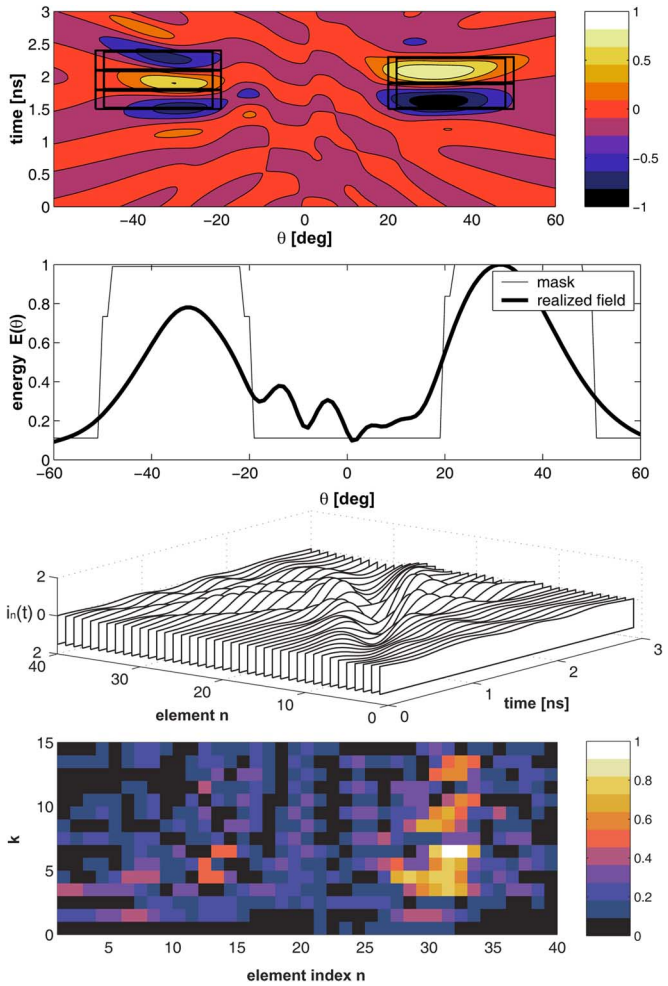

Fig. 16. Multi-beam pattern—Synthesis set-up: $d = 5\ \text{cm}$, $N = 40$, $K = 14$, $q = 1$, $\lambda = 0.55T_1$. Realized field and currents.

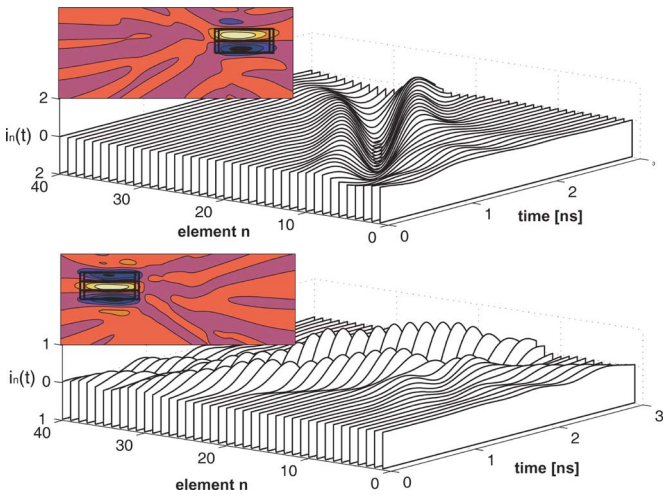

Fig. 17. Multi-beam pattern—Each beam independently synthesized, with the same parameters in Fig. 16.

The examples have demonstrated that the method is capable to generate both highly collimated beam as well as multibeam patterns wherein different field waveforms could be excited at different angular directions. The synthesis is as more effective

as the array antennas are less dispersive, but good results have been found also for broadband dipole-like impulse responses.

Further work will consider the extension of the method to planar and circular array configurations.

APPENDIX
CALCULATION OF $\mathcal{R}^{-1}$

The application of the alternate projection in the time domain requires the calculation of the inverse Radon transform of the projected array factor in $\mathcal{M}$ to find the mth estimation of the array current in (21). The application of the $\mathcal{R}^{-1}$ operator can be performed by means of a sequence of Fourier transforms in virtue of the Projection Slice Theorem [28]. This relates the Fourier transform of a projection of any function $f(z,t)$, e.g., its Radon transform $\mathcal{R}\circ f(z,t)$, to a *slice* of its two-dimensional Fourier transform [29], [30]

$$\mathcal{F}_{z\to\theta}\circ\mathcal{F}_{t\to\omega}\circ f(z,t)=\mathcal{F}_{t\to\omega}\circ[\mathcal{R}\circ f(z,t)] \tag{30}$$

where $\mathcal{F}_{a\to b}$ indicates the Fourier transform from the a-domain to the b-domain. For the specific application, the mth estimation of the array current source in (21) can be operatively performed as

$$i^{(m)}(z,t)=\mathcal{F}^{-1}_{\omega\to t}\circ\mathcal{F}^{-1}_{\theta\to z}\circ\mathcal{F}_{t\to\omega}\circ P_{\mathcal{M}}\circ AF^{(m)}(\theta,t). \tag{31}$$

Due to the linearity of all the considered operators, the previous expression may be rewritten by changing the orders of the Fourier transforms as

$$i^{(m)}(z,t)=\mathcal{F}^{-1}_{\omega\to t}\left[\mathcal{F}^{-1}_{\theta\to z}\circ P_{\mathcal{M}}\circ\widetilde{AF}^{(m)}(\theta,\omega)\right] \tag{32}$$

where $\widetilde{AF}^{(m)}(\theta,\omega)=\mathcal{F}_{t\to\omega}\circ AF^{(m)}(\theta,t)$ is the frequency domain array factor. It is worth noticing that the function within the square bracket is the conventional Fourier synthesis applied to the cropped array factor outside the mask.

ACKNOWLEDGMENT

The authors wish to thank Prof. O. M. Bucci for suggestions and valuable discussions.

REFERENCES

[1] C. E. Baum, "Transient arrays," in *Ultra-Wideband, Short-Pulse Electromagnetics 3*, C. Baum, L. Carin, and A. P. Stone, Eds. New York: Plenum Press, 1997, pp. 129–138.

[2] E. L. Mokole, "Behavior of ultrawideband-radar array antennas," in *Proc. IEEE Int. Symp. on Phased Array Systems and Technology*, 1996.

[3] F. Anderson, W. Christensen, L. Fullerton, and B. Kortegaard, "Ultrawideband beamforming in sparse arrays," *Proc. Inst. Elect. Eng. Bol.*, ser. H, vol. 138, no. 4, pp. 342–346, 1991.

[4] K. Siwiak and D. McKeown, *Ultra-Wideband Radio Technology*. New York: Wiley, 2004.

[5] M. Ghavami, L. B. Michael, and R. Kohno, *Ultra-Wideband Signals and Systems in Communication Engineering*. New York: Wiley, 2004.

[6] M. G. M. Hussain, "Principles of space-time array processing for ultrawide-band impulse radar and radio communications," *IEEE Trans. Veh. Technol.*, vol. 51, no. 3, pp. 393–403, 2002.

[7] A. Shlivinski and E. Heyman, "A unified kinematic theory of transient arrays," in *Ultra-Wideband Short-Pulse Electromagnetics 5*, P. D. Smith and S. R. Cloude, Eds. New York: Kluwer Academic/Plenum Publisher, 2000, pp. 327–334.

[8] J. L. Schwartz and B. D. Steinberg, "Ultrasparse, ultrawideband arrays," *IEEE Trans. Ultrason., Ferroelectr. Freq. Contr.*, vol. 45, no. 2, pp. 376–393, 1998.

[9] M. Ciattaglia and G. Marrocco, "Investigation on antenna coupling in pulsed arrays," *IEEE Trans. Antennas Propag.*, vol. 54, no. 3, pp. 835–843, 2006.

[10] W. Sorgel, C. Sturm, and W. Wiesbeck, "Impulse response of linear UWB antenna arrays and the application to beam steering," in *IEEE Int. Conf. on Ultra-Wideband*, 2005, pp. 275–280.

[11] A. Shlivinski and E. Heyman, "Discrete array representation of continuous space-time source distribution," *Turkish J. Elect. Eng.*, vol. 10, no. 2, pp. 257–271, 2002.

[12] E. Heyman and T. Melamed, "Certain considerations in aperture synthesis of ultrawideband/short-pulse radiation," *IEEE Trans. Antennas Propag.*, vol. 42, no. 4, pp. 518–525, 1994.

[13] D. M. Pozar, Y. Kang, D. H. Schaubert, and R. E. McIntosh, "Optimization of the transient radiation from a dipole array," *IEEE Trans. Antennas Propag.*, vol. 33, no. 1, pp. 69–75, 1985.

[14] Y. Kang and D. M. Pozar, "Optimization of pulse radiation from dipole arrays for maximum energy in a specified time interval," *IEEE Trans. Antennas Propag.*, vol. 34, no. 12, pp. 1383–1390, 1986.

[15] E. J. Bond, X. Li, S. C. Hagness, and B. D. V. Veen, "Microwave imaging via space-time beamforming for early detection of breast cancer," *IEEE Trans. Antennas Propag.*, vol. 51, no. 8, pp. 1690–1705, 2003.

[16] A. Shlivinski, E. Heyman, and R. Kastner, "Antenna characterization in the time domain," *IEEE Trans. Antennas Propag.*, vol. 45, no. 7, pp. 1140–1149, 1997.

[17] G. Beylkin, "Discrete Radon transform," *IEEE Trans. Acoust., Speech Signal Processing*, vol. 35, no. 2, pp. 162–172, 1987.

[18] O. M. Bucci, G. Franceschetti, G. Mazzarella, and G. Panariello, "Intersection approach to array pattern synthesis," *Proc. Inst. Elect. Eng.*, vol. 137, no. 6, pt. H, pp. 349–357, 1990.

[19] C. A. Balanis, *Antenna Theory: Analysis and Design*, 2nd ed. New York: Wiley, 1997.

[20] J. Rahman and T. Sarkar, "Deconvolution and total lest squares in finding the impulse response of an electromagnetic system from measured data," *IEEE Trans. Antennas Propag.*, vol. 43, pp. 416–421, 1995.

[21] G. Marrocco and F. Bardati, "Time-domain macromodel of planar microwave devices by FDTD and moment expansion," *IEEE Trans. Microw. Theory Tech.*, vol. 49, pp. 1321–1328, 2001.

[22] M. Ciattaglia and G. Marrocco, "Approximate calculation of time-domain effective height for aperture antennas," *IEEE Trans. Antennas Propag.*, vol. 53, pp. 1054–1061, 2005.

[23] L. R. L. Conte, R. Merletti, and G. V. Sandri, "Hermite expansions of compact support waveforms: Applications to myoelectric signals," *IEEE Trans. Biomed. Eng.*, vol. 41, no. 12, pp. 1147–1159, 1994.

[24] L. E. Miller, "Autocorrelation functions for Hermite-polynomial ultrawideband pulses," *Electron. Lett.*, vol. 39, no. 11, pp. 870–871, 2003.

[25] T. K. Sarkar and O. Pereira, "Using the matrix pencil method to estimate the parameters of a sum of complex exponentials," *IEEE Antennas Propag. Ma.*, vol. 37, no. 1, pp. 45–55, 1995.

[26] H. Achantz, "Time domain array design," in *Ultra-Wideband Short-Pulse Electromagnetics 5*. New York: Kluwer Academic /Plenum, 2002, pp. 385–392.

[27] G. Franceschetti, J. Tatojan, and G. Gibbs, "Timed arrays in a nutshell," *IEEE Trans. Antennas Propag.*, vol. 53, no. 12, pp. 4073–5082, Dec. 2005.

[28] R. M. Mersereau and A. V. Oppenheim, "Digital reconstruction of multidimensional signals from their projections," *Proc. IEEE*, vol. 62, no. 10, pp. 1319–1347, 1974.

[29] B. T. Kelley and V. K. Madisetti, "The fast discrete Radon transform-I: Theory," *IEEE Trans. Image Processing*, vol. 2, pp. 382–400, 1993.

[30] G. R. Ramesh, N. Srinivasa, and K. Rajgopal, "An algorithm for computing the discrete Radon transform with some applications," in *Proc. 4th IEEE Region 10 Int. Conf. TENCON'89*, 1989, pp. 78–81.

Matteo Ciattaglia received the Laurea in Telecommunication Engineering and the Ph.D. degree in geoinformation from the University of Rome "Tor Vergata," Rome, Italy, in 2002 and 2007, respectively.

In 2003, he was a Grant Researcher at the University of Rome "Tor Vergata," working on numerical methods for time-domain electromagnetics. He is currently employed at SELEX SI S.p.A., Rome, Italy, working on phased array modeling and design for radar systems. His research interests are in the area of time domain electromagnetics, UWB technology, numerical modeling, optimization methods, near field measurement techniques.

Dr. Ciattaglia received the "Mario Sannino" Award for the Best Scientific Presentation at the National Italian Congress of Electromagnetism (XV RiNEm) in 2004.

Gaetano Marrocco (M'98) received the Laurea in Electronic Engineering and the Ph.D. degree in applied electromagnetics from the University of L'Aquila, Italy, in 1994 and 1998, respectively.

Since 1997, he has been a Researcher at the University of Rome "Tor Vergata," Rome, where he currently teaches Antenna Design and Bioelectromagnetics. In summer 1994, he was at the University of Illinois at Urbana–Champain as a Postgraduate Student. In autumn 1999, he was a Visiting Researcher at the Imperial College, London, U.K. His research is mainly directed to the modelling and design of broad band and ultrawideband antennas and arrays as well as of miniaturized antennas for RFID applications. He has been involved in several space, avionic and naval programs of the European Space Agency, NATO, Italian Space Agency, and the Italian Navy. He holds two patents on broadband naval antennas and one patent on sensor RFID systems.

Prof. Marrocco currently serves as Associate Editor of the IEEE ANTENNAS AND WIRELESS PROPAGATION LETTERS.